Chapter 5. Non-Destructive Readout Ferroelectric Memories

This chapter is composed of three sections. In the first section, the current status of non-destructive readout ferroelectric memories is reviewed. Novel $A_2B_2O_7$ type ferroelectric materials are discussed in the second section. Finally, the preparation and properties of $Sr_2(Ta_{1-x}Nb_x)_2O_7$ solid-solutions are investigated as a function of composition in the last section.

5.1 LITERATURE REVIEW

As discussed in Chapter 1, the ferroelectric random access memory (FRAM) devices are divided into two categories, based on the readout technique: destructive read-out (DRO) and non-destructive read-out (NDRO). In the DRO FRAM device, reading operation is carried out destructively i.e. reversing the original polarization state, and reading the switching current. Therefore, reset procedures are required to restore the switched polarization state to the original position. On the other hand, the NDRO FRAM devices read the stored data by sensing the modulation of the surface conductivity of the silicon rather than switching the polarization state. This reading method provides a privilege of non-destructive readout and eliminates the reset procedure. The NDRO FRAM have several advantages of unlimited read cycles, fast speed, and strong potential for high packing density related to the 1 transistor cell format [1-2]. In particular, no fatigue in reading operation makes the NDRO FRAM devices superior to the DRO FRAM devices, which show the considerable fatigue problems.

The basic unit of the ferroelectric non-destructive readout (NDRO) device is 1 transistor (1T), which serves both as the storage element and the sensing device. The principal structures of NDRO device are divided into a metal-ferroelectric-semiconductor (MFS) and metal-ferroelectric-metal-insulator-semiconductor (MFMIS) structure [3-4]. Figure 5.1 illustrates cross section of the 1T memory cell using the MFS and MFMIS structure. The MFS structure, first developed by Wu [3], was almost identical to the standard silicon metal-insulator-semiconductor field effect transistor (MISFET), except that the insulator in MISFET was replaced by a thin layer of sputter-deposited ferroelectric bismuth titanate. The ferroelectric device using the MFS structure worked properly with good stability, but a very large switching voltage was required, which makes it incompatible with the existing silicon ICs. The ferroelectric memory capacitors are required to switch at an applied voltage of less than 5 V for being compatible with standard silicon CMOS technology. In addition, the device showed very slow speed (switching time of the order of microseconds), which was attributed to tunnel-injection effects. In the ferroelectric device using the MFS structure, the electrical charges were injected from the silicon surface into traps in the ferroelectric film through the thin native SiO_2 barrier layer, leading to injection type on/off switching instead of the polarization-type switching. The tunneling-trapping problem can be solved by using specific mandatory cleaning steps to remove the tunneling-trapping-barrier layer or preparing a thicker barrier layer as demonstrated by Buhay et al [5].

The current candidate materials for NDRO FRAM devices using MFS structure are $BaMgF_4$ and $Bi_4Ti_3O_{12}$ thin films, mainly investigated by Westinghouse [6-7]. The non-oxide $BaMgF_4$ films were grown on 4-in. diameter silicon wafers in a modified Vacuum Generators V80H molecular-beam epitaxy (MBE) system [6]. The high vacuum growth of this non-oxide films on a clean silicon substrate provides very low interface

a)

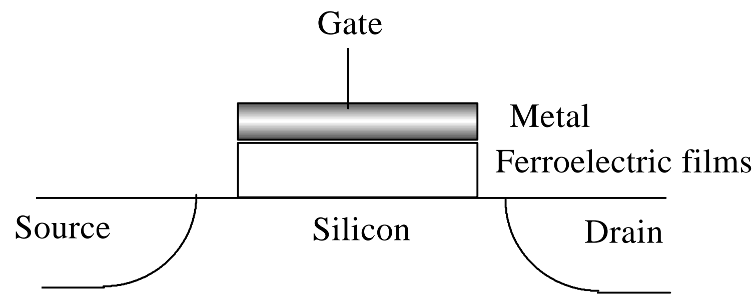

b)

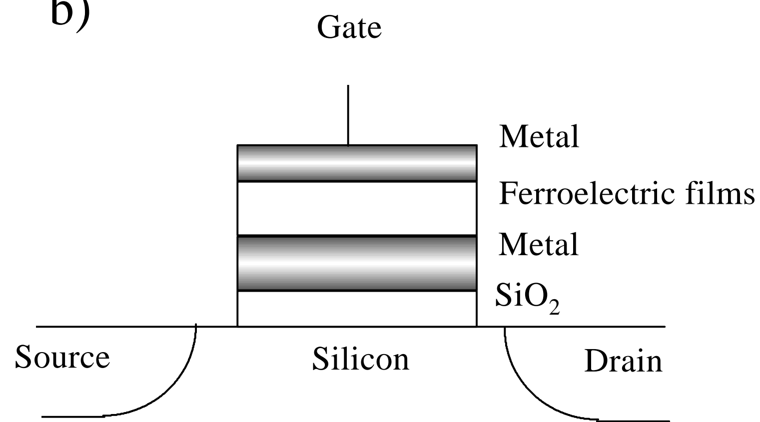

Figure 5.1 Schematic of 1-transistor memory cell using (a) MFS structure and (b) MFMIS structure.

state density, which is a critical requirement for the FET-type memory device structure. The polycrystalline films showed the spontaneous polarization value of 3.16 μC/cm^2 at 19.9 V, which is lower than the bulk value of 8.5 μC/cm^2 possible due to the random orientation. However, the commercialization of $BaMgF_4$ films for the NDRO FRAM devices are restricted due to high leakage current density and still due to high writing voltage. Another ferroelectric thin films material under study for developing the NDRO FRAM devices is $Bi_4Ti_3O_{12}$, which is deposited by pulsed laser deposition (PLD) [8]. Wu [3] used these films as the gate materials in the ferroelectric memory transistors, which showed the injection type on/off switching rather than the desired ferroelectric polarization switching. Buhay et al have reported to prevent the charge injection behavior by using a buffer layer of thermally grown SiO_2 as an injection barrier. The $Bi_4Ti_3O_{12}$ films prepared on the buffer barrier layers by pulse laser deposition technique exhibited good C-V hysteresis loop [8], indicating that the ferroelectric switching was dominant over the injection type switching by using the good quality SiO_2 layer for the injection barrier. These results suggest the possibility to integrate oxide films in the NDRO FRAM device structure.

The other cell structure for the NDRO FRAM device is metal-ferroelectric-metal-oxide-semiconductor (MFMIS) [4], which is very similar to the floating gate memory devices. The basic operating mechanism in the MFMIS structure is the same as in MFS structure. Since the oxide layer is incorporated into the cell structure, the injection effects are eliminated, as discussed in the MIS structure. However, the effective voltage applied to the films is very small due to high dielectric constant of the ferroelectric films. In the NDRO device using MFMIS structure, the ferroelectric films are connected to SiO_2 in series (Figure 5.1). When the voltage is applied to the gate, the voltage is divided into

ferroelectric (V_F) and SiO_2 capacitor (V_{ox}), and the charge stored in the device can be expressed as given in equations below.

$$V_T = V_{ox} + V_F$$

$$\varepsilon_F V_F t_{ox} = \varepsilon_{ox} V_{ox} t_F,$$

$$V_F = (\varepsilon_{ox}/\varepsilon_F)(t_F/t_{ox})\ V_{ox}$$

$$= [1/(1+(\varepsilon_F/\varepsilon_{ox})(t_{ox}/t_F))]\ V_T$$

The effective voltage applied to the ferroelectric films is reduced by the ratio of dielectric constant of SiO_2 and ferroelectric films. Considering the typical dielectric constant (800 - 1000) of the ferroelectric films, the effective voltage becomes too small for polarization switching. Thus, in order to apply sufficient voltage for polarization to the ferroelectric films, the dielectric constant should be fairly small. The low dielectric constant is also required for the ferroelectric memory devices using the MFS structure. The applied electric field of the MFS structure is expressed as $E_F = E_A - P/\varepsilon_0$, where E_A, P, and ε_0 mean applied electric field, polarization, and dielectric permittivity of vacuum, respectively. Since the polarization of the films is proportional to the dielectric constant, when the ferroelectric films exhibit large dielectric constant, the value of polarization was increased, which results in lowering the actual electric field applied to the ferroelectric films. The term of P/ε_0 is called as depolarization electric field. Therefore, in order to achieve sufficient electric field for switching the polarization, the ferroelectric films used in the MFS structure should possess low dielectric constant for reducing the depolarization electric field.

While $BaMgF_4$ and bismuth titanate have been prepared on the MFS structure, $Pb(Zr_{1-x}Ti_x)O_3$ and $PbTiO_3$ have been fabricated on the MFMIS structure [3-4,8]. In the

MFS structure, the oxide ferroelectric films react with silicon and form an undesired interfacial layer, which deteriorates the device performance severely. Thus, an insulating layer such as SiO_2 and metal layer are inserted between the ferroelectric films and the silicon, giving rise to the MFMIS structure. In this case, no undesired reaction occurs between ferroelectric films and silicon, but the effective voltage applied to the films is very small due to high dielectric constant of the ferroelectric films. Therefore, ideal ferroelectric materials for the NDRO device should possess low dielectric constant, low coercive electric field, low leakage current density, and just sufficient remanent polarization to cause the modulation of the silicon surface conductivity. Therefore, it is desirable to develop a ferroelectric material with low dielectric constant and low coercive electric field. Among many oxide ferroelectric materials, $A_2B_2O_7$ type materials are reported to show extremely high Curie-temperature and low ε_r. In particular, $Sr_2Nb_2O_7$ single crystal exhibits low ε_r (60) and low E_c (6 kV/cm) [9], which satisfy the requirements for the NDRO device. In addition, solid-solution $Sr_2(Nb_xTa_{1-x})_2O_7$ also shows good electrical properties for the NDRO application, and their Curie-temperatures decrease as a function of Ta content [10]. In this study, we develop the novel ferroelectric thin films and investigate the structural and electrical properties of the films for NDRO device application.

5.2 $A_2B_2O_7$ FERROELECTRIC MATERIALS

5.2.1 Overview

In recent decades, $A_2B_2O_7$ compounds have received much interest , because of their complex structures, outstanding thermal stability, and extremely high Curie-temperature. Their crystal structures are typically characterized by perovskite-like slabs,

which are composed of corner-shared BO_6 octahedra and A cation coordinated with 12 oxygen. Figure 5.2 shows the unit cell of $A_2B_2O_7$ [11]. Among these perovskite-like $A_2B_2O_7$ compounds, strontium niobate ($Sr_2Nb_2O_7$) and lanthanum niobate ($La_2Ti_2O_7$) have been extensively investigated due to their excellent electrical properties and complex structural transition [9,12-13].

It has been reported that $Sr_2Nb_2O_7$ (SNO) shows three successive phase transition temperatures. The single crystal is orthorhombic at room temperature with a space group of $Cmc2_1$. The structure of strontium niobate changes from space group of Cmcm to $Cmc2_1$ at ferroelectric phase transition temperature, 1342 °C. Then, the incommensurate phase transition occurs at 215 °C [14]. Third phase transition is observed at -156 °C by an anomaly of the dielectric constant along the b-axis and by an anomaly of a soft-mode. The structure of $La_2Ti_2O_7$ (LTO) has two modifications at room temperature, one with a space group P_{21}, and the other with $Pbn2_1$. The structure transforms to orthorhombic space group, $Cmc2_1$ at around 780 °C, and then at 1500 °C, transforms into the paraelectric structure with a space group, Cmcm [15].

Being ferroelectric at room temperature, the single crystals of $Sr_2Nb_2O_7$ and $La_2Ti_2O_7$ exhibit high Curie-temperatures and possess excellent piezoelectric and electro-optic properties. It was also reported that single crystal $Sr_2Nb_2O_7$ and $La_2Ti_2O_7$ films could be used for thin film optical waveguide [16]. These useful properties make them strong candidates for a wide variety of electrical applications such as high temperature transducers and new optical devices. However, most of the studies on $Sr_2Nb_2O_7$ and $La_2Ti_2O_7$ material have been carried out using single crystal grown from float zone techniques. It is impractical to use single crystals in most of the electrical devices, because of the economic constrains of obtaining high quality specimens. Therefore, it is desired to fabricate $Sr_2Nb_2O_7$ and $La_2Ti_2O_7$ ceramics and thin films for practical applications.

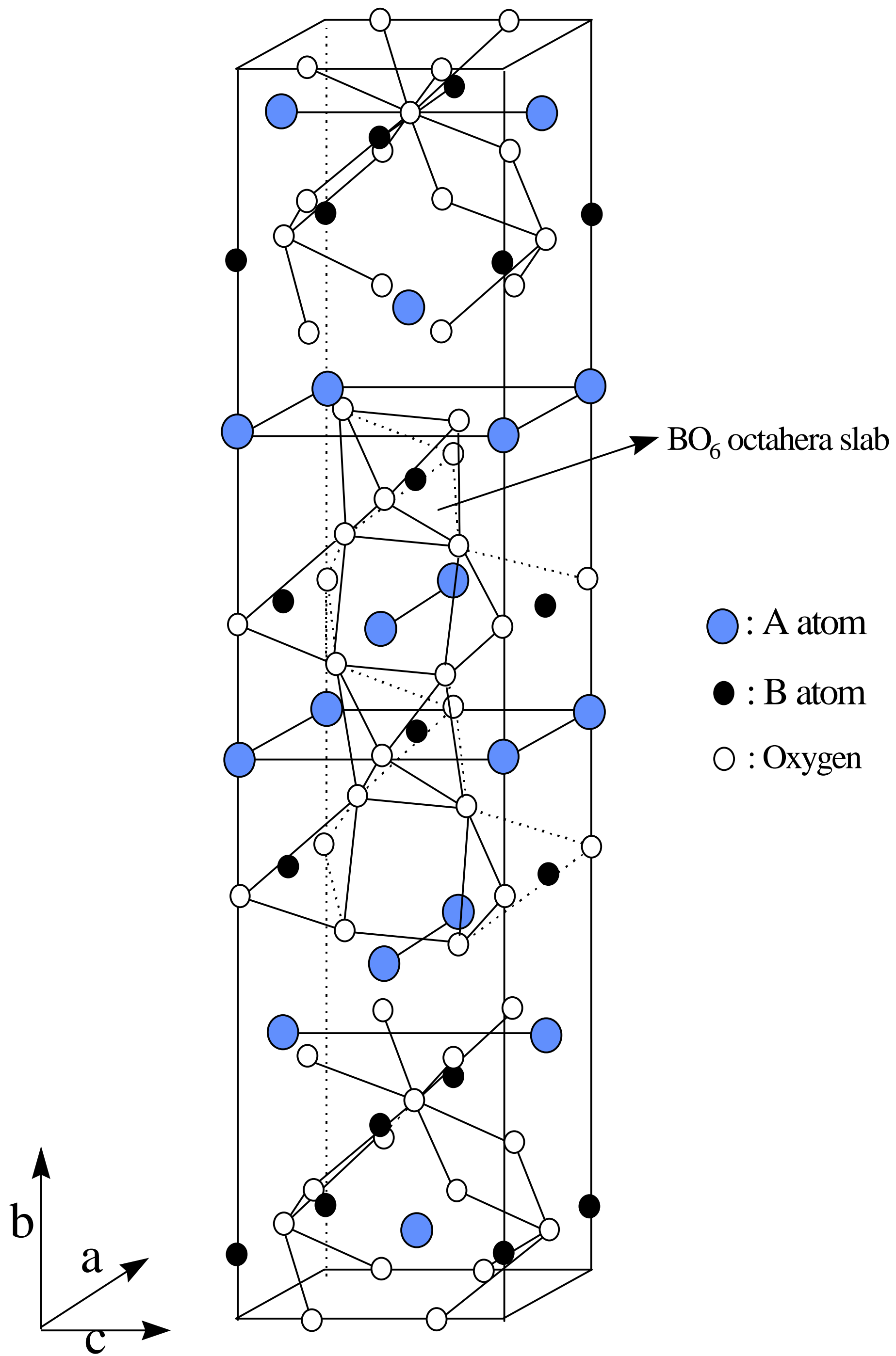

Figure 5.2 Unit cell of $A_2B_2O_7$.

$La_2Ti_2O_7$ and $Sr_2Nb_2O_7$ ceramics have been prepared by several processing techniques, including conventional powder mixing technique, molten salt synthesis technique, and sol-gel technique. The $La_2Ti_2O_7$ and $Sr_2Nb_2O_7$ ceramics have been reported to exhibit good density and dielectric properties compared to the single crystal. However, the preparation and electrical properties of $La_2Ti_2O_7$ and $Sr_2Nb_2O_7$ thin films were not sufficiently investigated. In this work, $La_2Ti_2O_7$ and $Sr_2Nb_2O_7$ thin films are prepared on Pt-coated silicon, Si(100), and $Pt/IrO_2/SiO_2/Si$ substrates by metalorganic deposition (MOD) technique, and their structural and electrical properties are primarily investigated.

The MOD technique has several advantages over other vacuum methods [17]: better control of stoichiometry, low processing temperature, simple equipment, low cost. Since the starting materials for the MOD process are mixed on the molecular level, the inorganic components are intimately contacted as atoms or molecules after decomposition. This creates much faster formation of compounds, which results in lower processing temperature. Furthermore, MOD method is compatible with ultra large scale integral (ULSI) circuit because of uniform film deposition over large areas.

5.2.2 Experimental Procedures

5.2.2.1 Precursors selection

It is required that ideal metalorganic precursors for the MOD process posses the following properties: high metal component; high solubility in common organic solvents; stability under ambient conditions (e.g., should not gel); thermal decomposition without melting or evaporating; and compatibility with other compounds in the formulation. However, all of the desired properties cannot be simultaneously satisfied. For example, the solubility is enhanced by increasing the chain length of organic ligand, but the metal

content is reduced as the chain length increases. Therefore, the starting materials selected in this experiment were compromised among these various requirements.

5.2.2.2 Sample preparation

For preparing the $La_2Ti_2O_7$ thin films, lanthanum 2-ethylhexanoate ($La(OOCC_7H_{15})_3$, Chemat Tech. Inc., 99.9%), titanium ethoxide ($Ti(OC_2H_5)_4$, 99.9%, Aldrich), and 2-ethylhexanoic acid ($CH_3(CH_2)_3CH(C_2H_5)CO_2H$, Aldrich) were chosen as the starting materials, and xylene ($C_6H_4(CH_3)_2$, Aldrich) as the solvent. First, titanium ethoxide was mixed with 2-ethylhexanoic acid in xylene, and was stirred for 30 min at 100 ~ 120 °C. Lanthanum 2-ethylhexanoate was added to the solution, which was stirred at 120 ~ 140 °C until the final concentration of the solution was 0.1 mole/liter. In the $Sr_2Nb_2O_7$ cases, all preparation steps are the same as observed in the LTO films. Only precursors and solvent are different from the LTO films preparation. Strontium 2-ethyl hexanoate ($Sr(C_7H_{15}COO)_2$, 99.8%, Alfa), niobium ethoxide($Nb(OC_2H_5)_5$, 99.95%, Aldrich), and 2-ethylhexanoic acid ($C_7H_{15}COOH$, 99%, Aldrich) were used as the starting materials, and butyl acetate as the solvent. The final concentration of the solution was 0.1 moles/liter. These solutions were filtered using a filter with 0.25 μm pore size to remove particulate impurities. These solutions were used to deposit $La_2Ti_2O_7$ and $Sr_2Nb_2O_7$ thin films on Si(100) and $Pt/Ti/SiO_2/Si$ using spin-coating technique. Before the spin-coating deposition, the substrates were cleaned by immersion in acetone, ethanol and distilled water, then dried with nitrogen. This cleaning process was found to enhance the film adhesion to the substrate and the film quality. The solution was deposited onto the substrates which were rotated at 4000 rpm for 40 sec. Then, the as-coated films were baked on a hot plate at 200 °C. The spin-bake process was repeated until the desired film thickness was obtained. The dried films were pyrolyzed at 450 °C in oxygen atmosphere

to convert the metalorganic precursors to oxides or their constituent elements. The pyrolysis temperature was determined by thermogravimetric analysis (TGA) results which showed that at around 400 °C most of 2-ethylhexanoate groups were evaporated from the sample. The pyrolyzed films were finally annealed at various temperatures ranging form 650 to 850 °C for crystallization. The final thickness of the film after annealing was measured by ellipsometry as 0.4 μm. Figure 5.3 shows flow chart of all the steps used in the fabrication of $La_2Ti_2O_7$ and $Sr_2Nb_2O_7$ thin films.

5.2.2.3 Sample characterization

The structure of the films was characterized by using x-ray diffraction (XRD) patterns, which were recorded on a Scintag XDS 2000 diffractometer using CuK radiation at 40 kV. The microstructure of the films was characterized by using Digital Instrument's Dimension 3000 atomic force microscope (AFM) using tapping mode with amplitude modulation.. The electrical measurements were conducted on films in metal-ferroelectric-metal (MFM) configuration. The MFM capacitors were fabricated by depositing Pt top electrodes of an area $2.1X10^{-4}$ cm^2 on the surface of the films using a shadow mask by rf sputtering. The dielectric measurement were carried out by using HP4192A impedance analyzer.

5.2.3 Results

The X-ray diffraction (XRD) patterns were observed for the $Sr_2Nb_2O_7$ and $La_2Ti_2O_7$ films annealed at various temperatures ranging from 650 to 850 °C. Figure 5.4 shows the phase development of $Sr_2Nb_2O_7$ film prepared on Pt-coated silicon and Si(100) substrates. Polycrystalline $Sr_2Nb_2O_7$ films were observed at an annealing temperature of

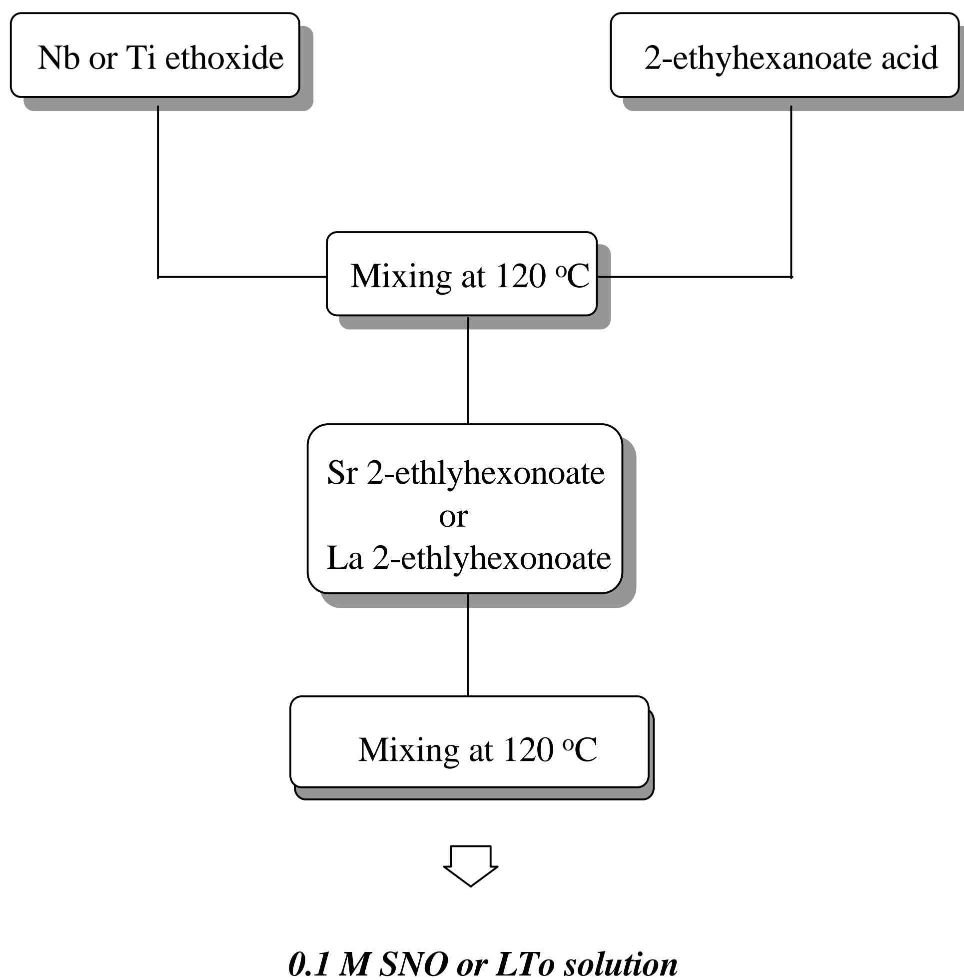

Figure 5.3 Flow chart of preparing SNO and LTO solutions.

850 °C via intermediate phase whose composition is close to $Sr_{0.8}NbO_3$. In the XRD patterns of $Sr_2Nb_2O_7$ ceramics fabricated by conventional method, very strong (080) peaks were observed, which indicated the sample was highly grain-orientated along (0k0) direction. However, the $Sr_2Nb_2O_7$ thin films annealed at 850 °C illustrated (131) peak as highest intensity peak in Figure 5.4, and the grain orientation along (0k0) direction was not obvious in the XRD patterns of the thin films. Instead, the patterns were similar to those of $Sr_2Nb_2O_7$ powders calcined at 1100 °C using conventional powder mixing method. The match of calcined powders and annealed thin films in XRD patterns indicated that the grains were randomly oriented rather than growing along a specific direction.

Figure 5.5 shows the XRD patterns of the $La_2Ti_2O_7$ films on Si(100) and Pt-coated Si substrates. The $La_2Ti_2O_7$ films were completely crystallized in the single phase at around 750 °C without any intermediate phase formation as verified from the Joint Commission on Powder Diffraction Standards (JCPDS) file no. 28-517. As the annealing temperature was increased, the intensity of the XRD peaks was enhanced due to further crystallization and grain growth. The single phase of the films was found to be similar to that of $La_2Ti_2O_7$ bulk ceramics, but the films displayed no preferred orientation which was also observed in the bulk ceramics. The XRD peaks of the films matched very well with respect to relative intensity and diffraction angle with those of $La_2Ti_2O_7$ powders calcined at 1200 °C synthesized by using conventional powder processing technique. The XRD matching indicated the random grain orientation of $La_2Ti_2O_7$ thin films.

Figure 5.6 shows the microstructures of the $Sr_2Nb_2O_7$ films on Pt-coated silicon substrates annealed at 850 °C. No cracks or voids were observed in the annealed films. The films appeared to have a homogeneous microstructure with a fine grain size of around 0.3 μm. The grains appeared elongated , but actually the shape of grains was slab type. The grains were orientated randomly on the surface of the films. Very uniform films were

(a)

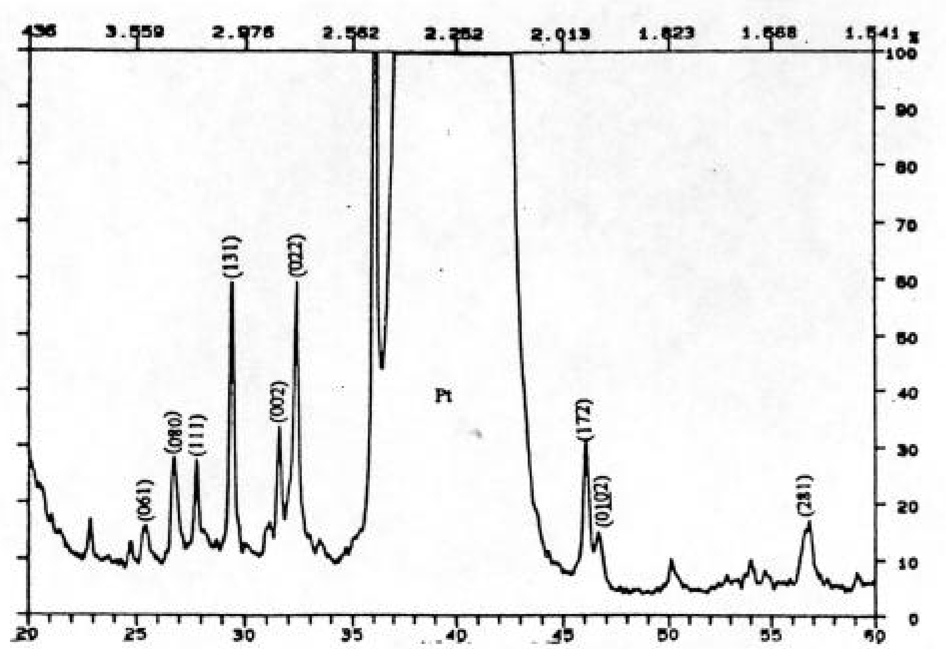

(b)

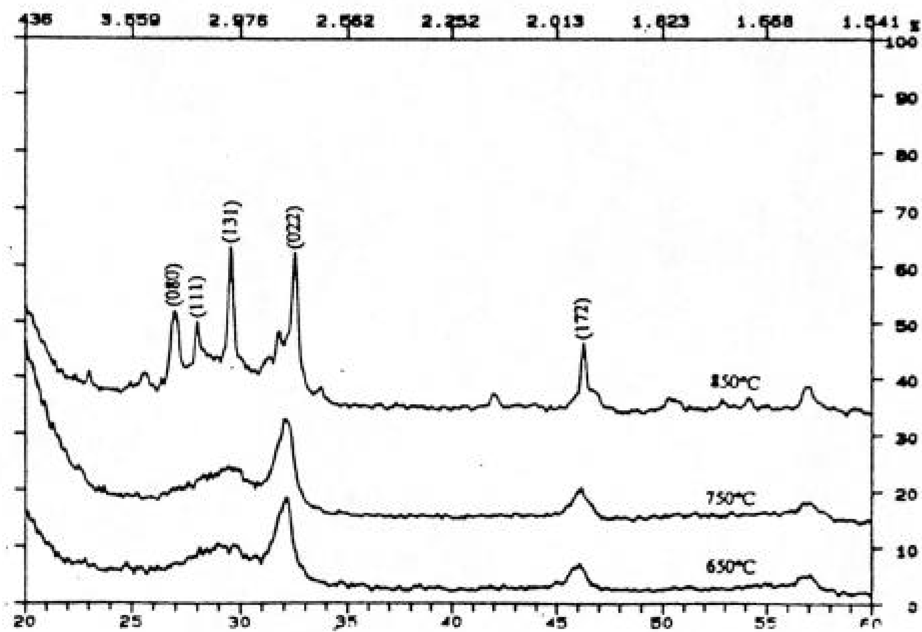

Figure 5.4 XRD patterns of SNO films on (a) $Pt/Ti/SiO_2/Si$ at 850 °C and (b) Si(100) substrates at various temperatures.

(a)

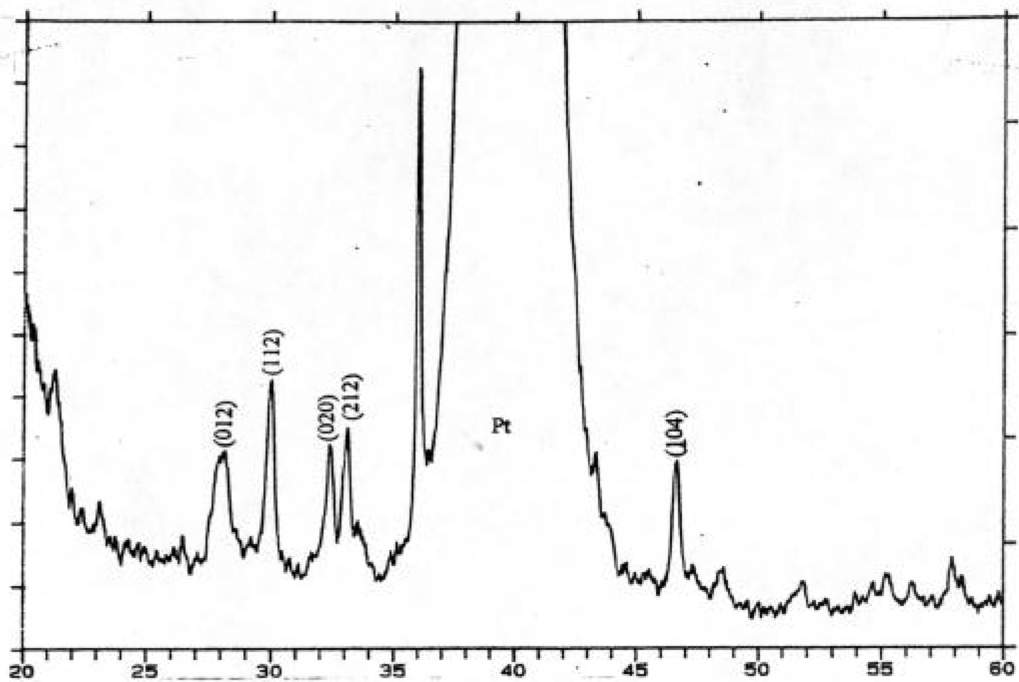

(b)

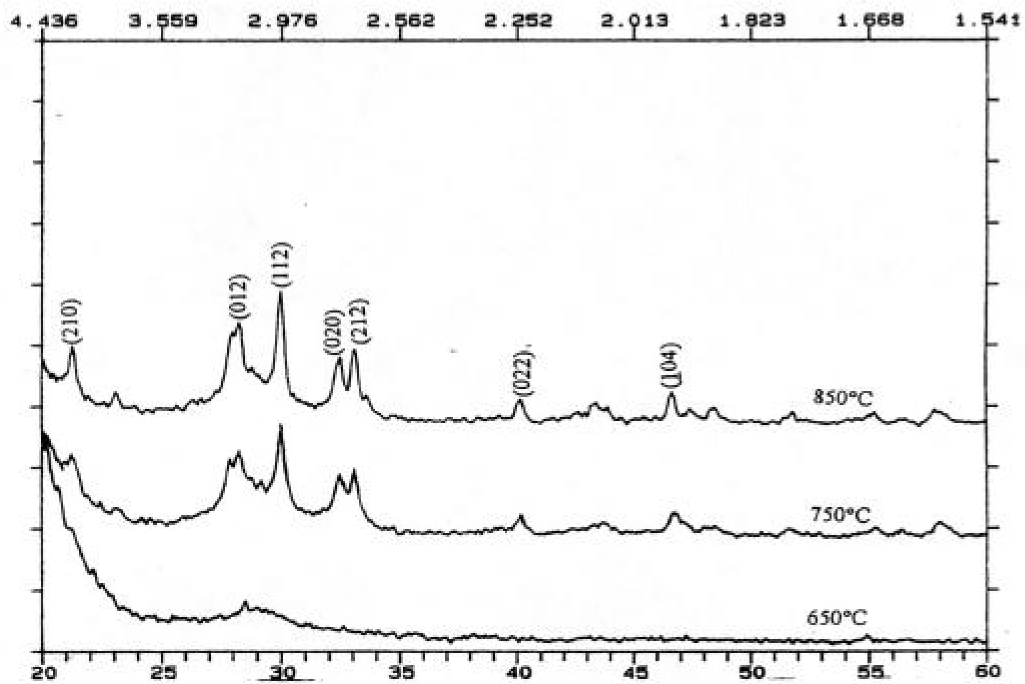

Figure 5.5 XRD patterns of LTO films on (a) $Pt/Ti/SiO_2/Si$ at 850 °C and (b) Si(100) substrates at various temperatures.

obtained with surface roughness of 50 nm. Figure 5.7 shows the surface microstructures of $La_2Ti_2O_7$ films deposited on Si(100) and Pt coated Si substrates. From these micrographs, it was observed that the grains were randomly distributed, and there was no substrate effect. The grains had rod-like shape with an average grain size of 50 nm.

The dielectric properties of the $Sr_2Nb_2O_7$ and $La_2Ti_2O_7$ films were analyzed in terms of the dielectric constant, ε_r, and dissipation factor, $\tan\delta$. Figure 5.8 (a) and (b) illustrate the dielectric constant and the dissipation factor as a function of frequency for these films annealed at 850 °C. For $Sr_2Nb_2O_7$ thin films, the values of dielectric constant and dielectric loss at a frequency of 100 kHz were 48 and 0.042, respectively. The values were found to be relatively unchanged up to a frequency of 5 MHz, and were close to those of $Sr_2Nb_2O_7$ bulks. In the case of $La_2Ti_2O_7$ thin films, the dielectric constant and dielectric loss at a frequency of 100 kHz were 45 and 0.040, respectively, comparable to those of $La_2Ti_2O_7$ bulks. The values were relatively unchanged up to a frequency of 5 MHz. Well-defined hysteresis loops were not observed for $Sr_2Nb_2O_7$ and $La_2Ti_2O_7$ film on Pt-coated silicon substrates, which might be attributed to the small grain size.

5.2.4 Summary

$La_2Ti_2O_7$ and $Sr_2Nb_2O_7$ thin films were successfully prepared on Pt-coated silicon and Si (100) substrates by a metalorganic deposition (MOD) technique. Randomly oriented polycrystalline $Sr_2Nb_2O_7$ films were formed at an annealing temperature of 850 °C through an intermediate phase whose composition was close to $Sr_{0.8}NbO_3$. On the other hand, the crystalline $La_2Ti_2O_7$ films were successfully obtained without any intermediate phase formation on Pt-coated silicon and bare silicon substrates at an annealing temperature of 750 °C. The surface microstructures of these films showed extremely fine and rod-like grains. The electrical characteristics of the films indicated that the dielectric

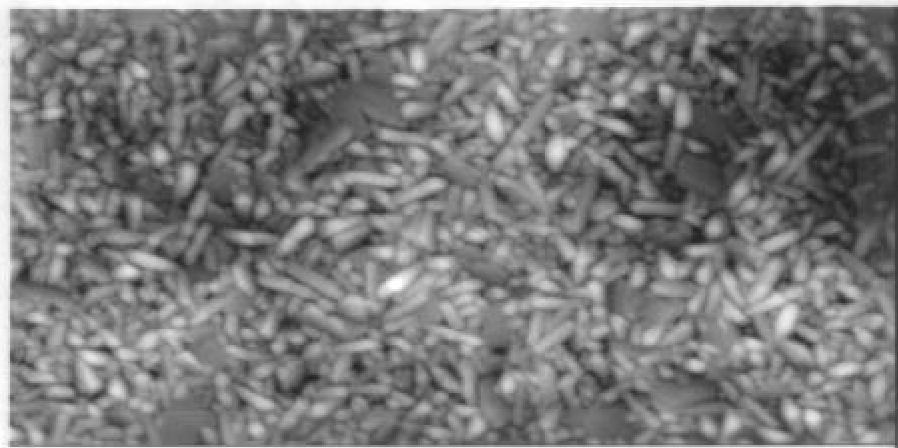

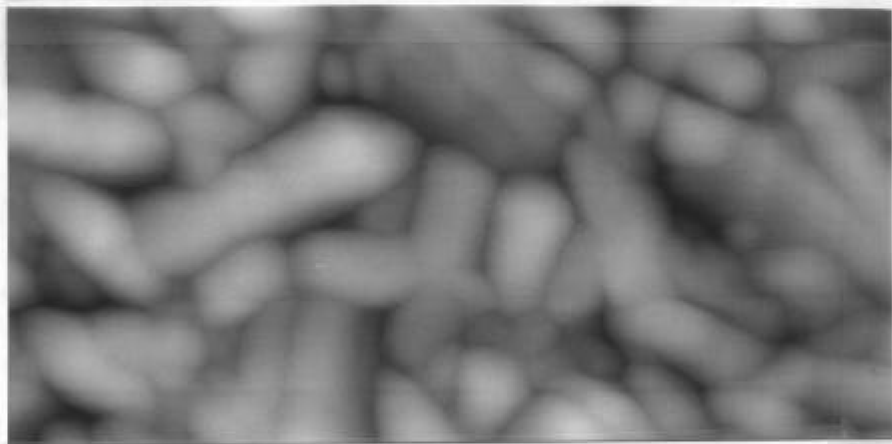

Figure 5.6 AFM pictures of SNO films on $Pt/Ti/SiO_2/Si$ at 850 °C.

(a)

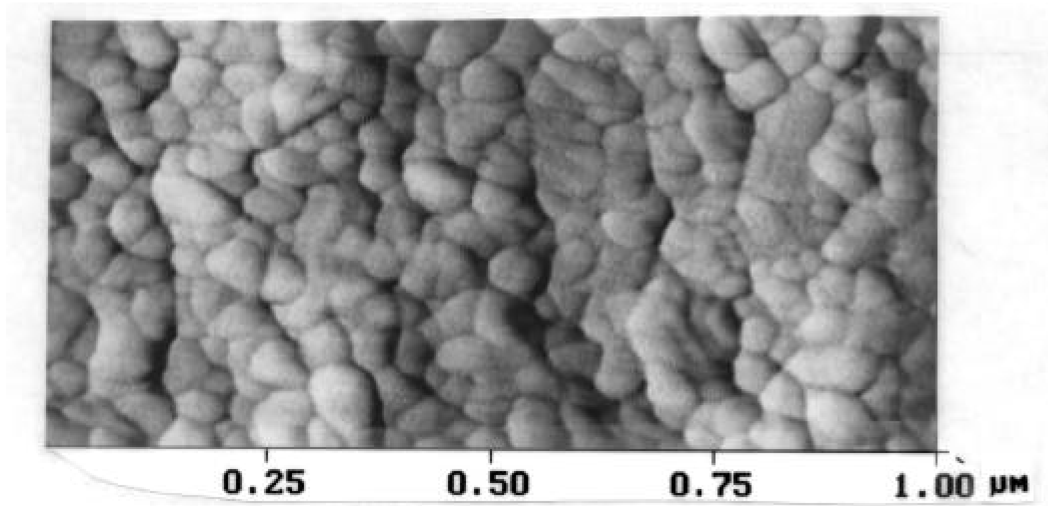

(b)

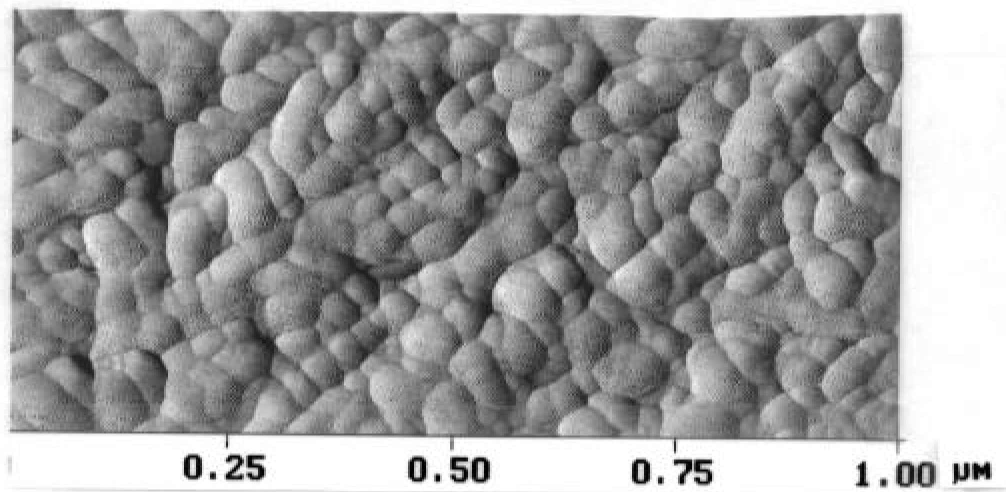

Figure 5.7 AFM pictures of LTO films on (a) Pt/Ti/SiO_2/Si at 850 °C and (b) Si(100) substrates at 850 °C.

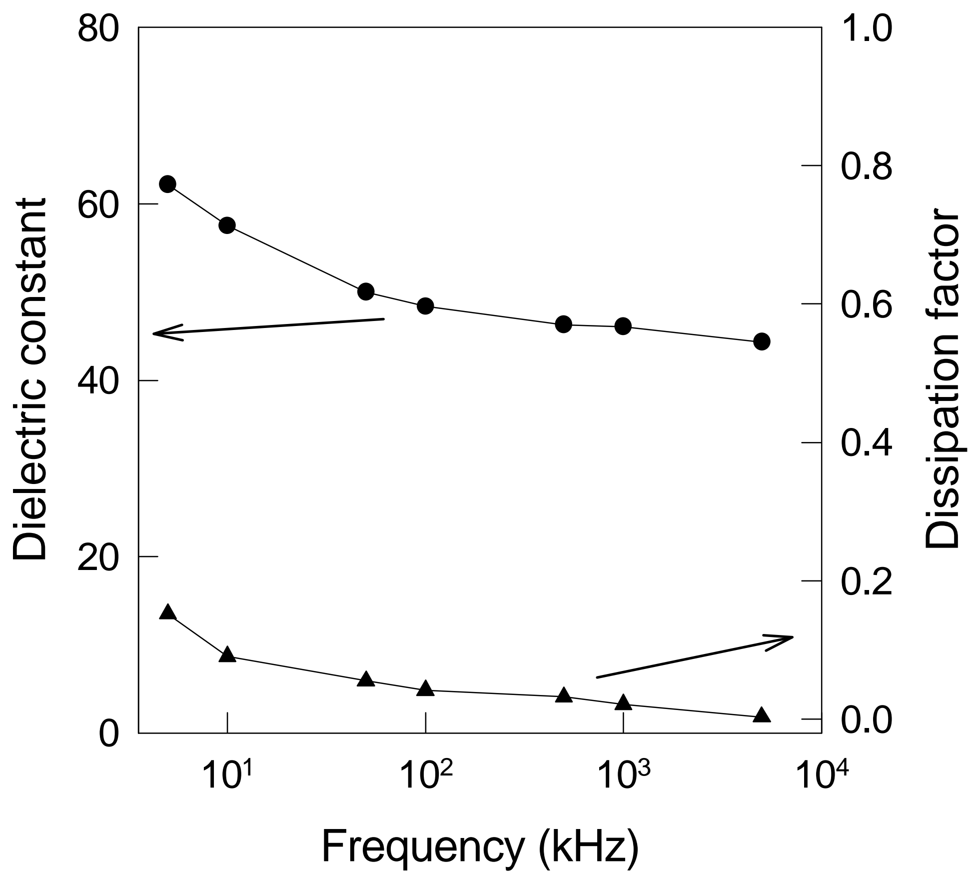

Figure 5.8 (a) Dielectric properties of SNO films on Pt/Ti/SiO_2/Si at 850 °C.

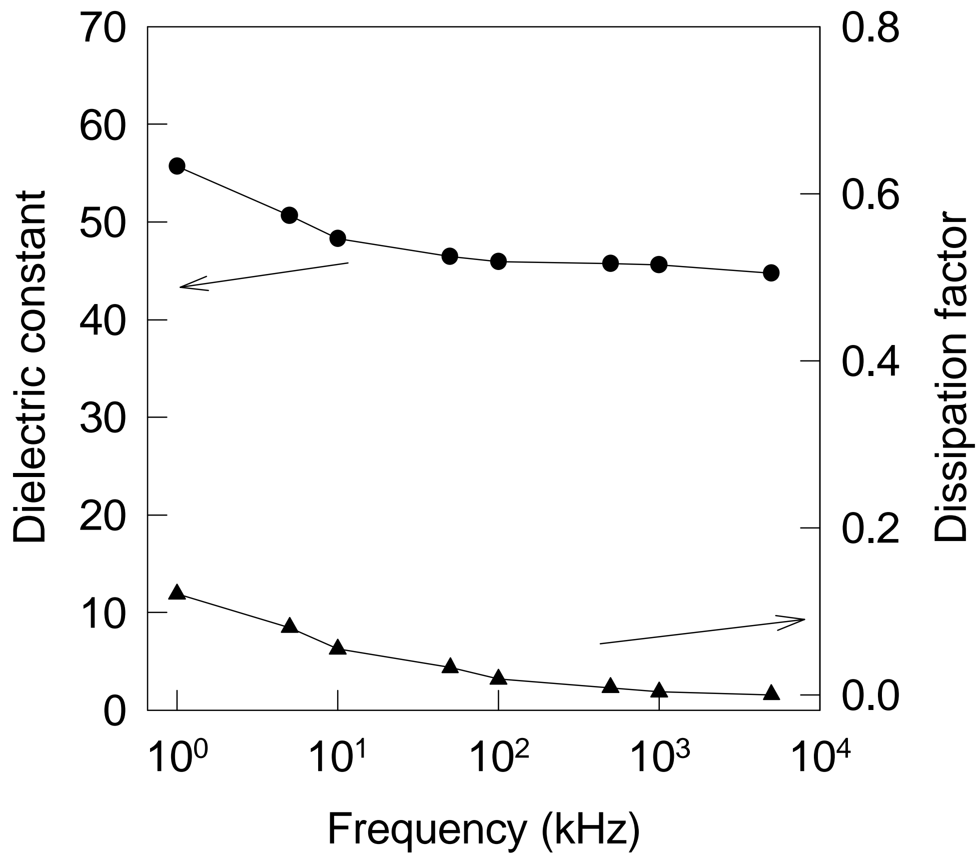

Figure 5.8 (b) Dielectric properties of LTO films on $Pt/Ti/SiO_2/Si$ at 850 °C.

properties of the films were relatively independent on signal frequency up to 5 MHz. The $Sr_2Nb_2O_7$ films exhibited the dielectric constant and dissipation factor at a frequency of 100 kHz as 48 and 0.0042, respectively, while $La_2Ti_2O_7$ films showed the ε_r and tan δ values as 45 and 0.040, respectively. Well-defined hysteresis loops were not observed for these films, which might be attributed to the extremely small grains.

5.3 $Sr_2(Ta_{1-x}Nb_x)_2O_7$ SOLID-SOLUTIONS

In order to investigate the structural and electrical properties of $Sr_2(Ta_{1-x}Nb_x)_2O_7$ (STN) solid solutions, first, STN bulk ceramics were fabricated using conventional powder mixing method. The STN thin films were then prepared on Pt-coated Si, Si(100), and $Pt/IrO_2/SiO_2/Si$ substrates by a metalorganic deposition (MOD) technique.

5.3.1 $Sr_2(Ta_{1-x}Nb_x)_2O_7$ Bulk Ceramics

Strontium tantalate ($Sr_2Ta_2O_7$) and strontium niobate ($Sr_2Nb_2O_7$) belong to $A_2B_2O_7$ type ferroelectric materials, which have perovskite-like structure [9,12]. Strontium niobate has been widely investigated, because the single crystal exhibits an extraordinarily high Curie-temperature, and excellent piezoelectric and electro-optical properties [11]. At room temperature, the crystal structure of $Sr_2Nb_2O_7$ is orthorhombic with the space group C_{2v}-$Cmc2_1$ [11]. $Sr_2Ta_2O_7$ has shown crystallographic properties very similar to strontium niobate, except very low ferroelectric phase transition temperature (-107 °C) [10]. The single crystal of $Sr_2Ta_2O_7$ is orthorhombic with D_{2h} space group and paraelectric at room temperature. Nanamatsu et al. [10] reported the $Sr_2(Ta_{1-x}Nb_x)O_7$ (STN) solid solutions and their Curie-temperatures, which varied drastically from -107 to 1342 °C as the Nb composition (x) increased from 0 to 1. They suggested that the

partial replacement of Ta element by Nb element changed the electronic polarizability of the cation in the oxygen octahedra, causing the ferroelectric phase transition temperature to drastically increase up to a high temperature.

Even though the Curie-temperatures of the STN solid solutions were examined, the STN powders and ceramics were not sufficiently investigated as a function of composition x. In this experiment, the STN ceramics were fabricated as a function of composition x using conventional powder mixing method. The structural and electrical properties of STN ceramics were systematically investigated as a function of composition x.

5.3.1.1 Sample preparation

The STN ceramics were prepared by conventional powder mixing (CON) method. Reagent-grade $SrCO_3$, Ta_2O_5 and Nb_2O_5, in appropriate molar ratio were mixed for 12 hours in crucible including alcohol and alumina media. The resulting slurry was dried at 150 °C to evaporate the alcohol, and then calcined at the temperature ranging from 600 to 1300 °C to obtain the single phase formation. Ceramics samples were prepared from $Sr_2(Ta_{1-x}Nb_x)_2O_7$ powders by adding 3 wt% binder, pressing into pellets with diameters of 15 mm at 98 MPa, and then sintering on zirconia setters at the temperature ranging from 1200 to 1500 °C.

The structure developments of the calcined powders and the sintered pellets were investigated by x-ray diffraction (XRD) patterns, which were recorded on Philip PW1840 diffractometer using CuKα radiation. The surface morphologies of the sintered bulk ceramics were investigated by using scanning electron microscopy (SEM). Bulk density of the sintered pellets was measured by the Archimedes method. The dielectric properties of the sintered pellets were measured in terms of the dielectric constant ε_r, and dissipation

factor tanδ. The dielectric measurements were carried out at room temperature by using an HP 4192A impedance analyzer. For electrical measurements, gold electrodes were deposited by RF sputtering on the top surface of the samples.

5.3.1.2 Results

Figure 5.9 illustrates the XRD patterns of $Sr_2(Ta_{1-x}Nb_x)_2O_7$ ceramics sintered at 1500 °C for various composition of x by using conventional powder mixing (CON) method. As the compositional ratio x varied from 0 to 1.0, the (080) peak increased and became dominant. The increase in (080) peak as a function of composition x is clearly observed in Figure 5.10, which shows XRD patterns particularly between 24 °and 34 °of 2θ values. The (080) peak was intensely developed as the Nb composition increased from 0 to 1.0. The extent of grain orientation was quantified in terms of the Lotgering orientation factor, f, which is defined as following equation given below [18]. In this study, XRD lines between 20 °and 60 °of 2θ values were used, as shown in Figure 5.9 for the estimation of grain orientation.

$$f = (p-p_0)/(1-p_0)$$

where $p = \sum\{0k0\}/ \sum\{hkl\}$ for the $Sr_2Nb_2O_7$ sintered pellet, $p_0 = \sum\{0k0\}/ \sum\{hkl\}$ for the $Sr_2(Ta_{1-x}Nb_x)_2O_7$ powder calcined at 1100 °C and f varies from 0 to 1. The grain orientation factor (f) of $Sr_2(Ta_{1-x}Nb_x)_2O_7$ ceramics was investigated for various composition, and shown in Figure 5.11. The grain orientation factor (f) was found to increase as a function of the composition, x. When the x increased from 0 to 1, the value of grain orientation factor drastically increased from 0.01 to 0.34. Typical characteristics of STN ceramics fabricated by the CON method are summarized in Table 2, in which the Curie-temperature and grain orientation was proportional to the compositional ratio x.

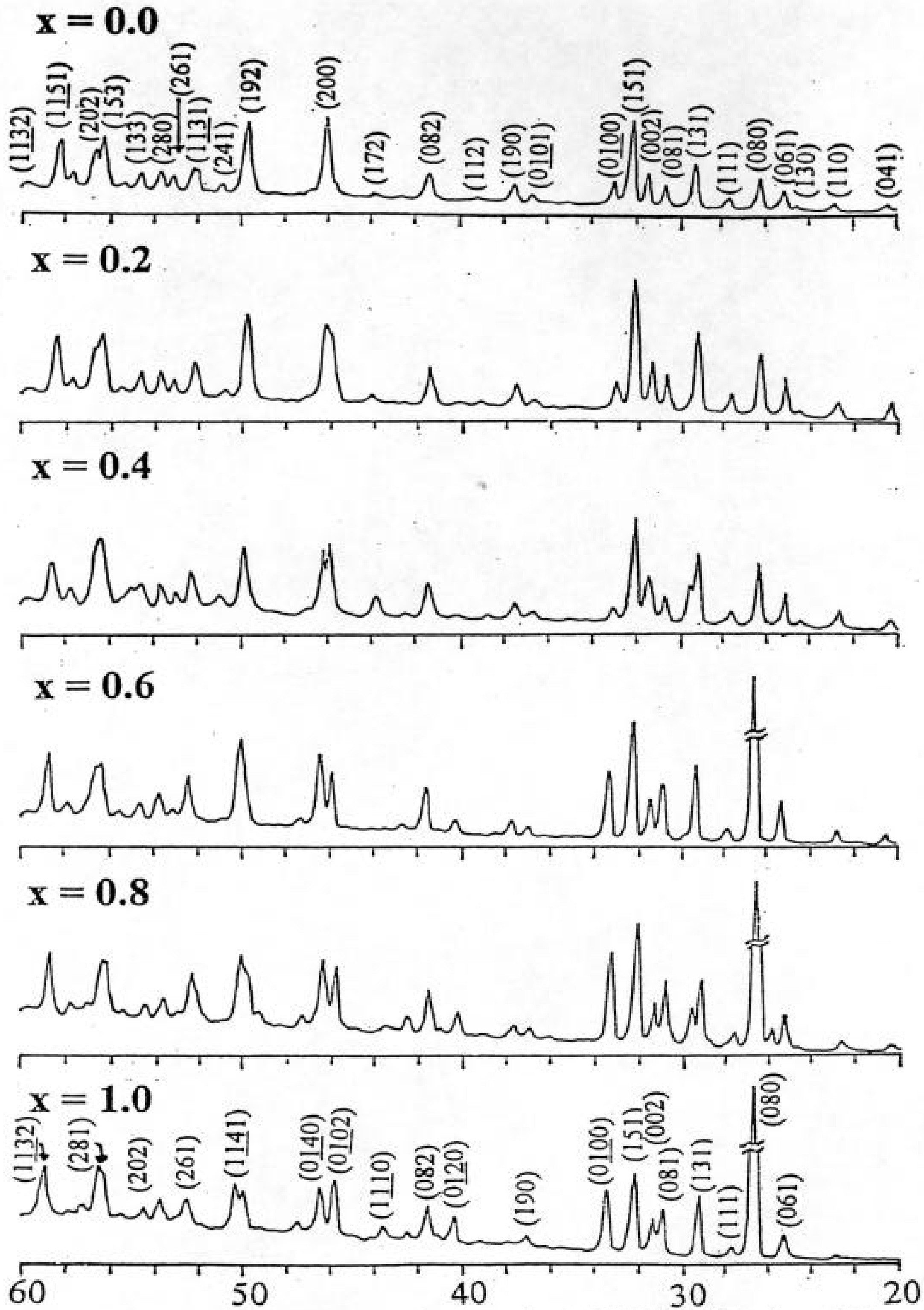

Figure 5.9 XRD patterns of STN ceramics sintered at 1500 °C as a function of Nb content.

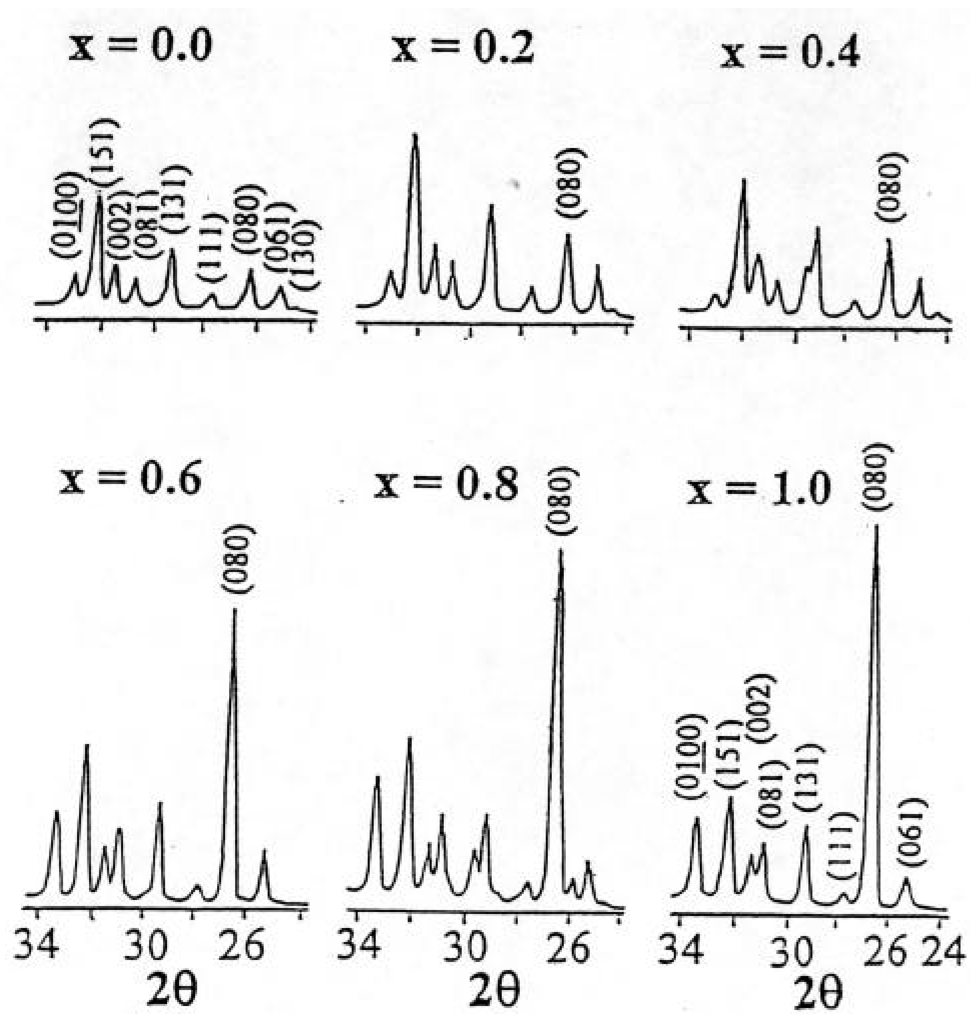

Figure 5.10 XRD patterns of STN ceramics sintered at 1500 °C.

For surface morphology studies, the sintered samples were polished and thermally etched by annealing the samples at 1400 °C for 10 min. Figure 5.12 shows SEM micrographs of STN ceramics as a function of composition x. The slab-type grains were observed, and the grain orientation and grain size increased with the increase of the composition x, as observed in XRD studies. Figure 5.11 illustrates the dependence of grain orientation and grain size on the composition x.

Table 5.1 summarizes the characteristics of the STN ceramics fabricated by the CON method. Dielectric constants at room temperature for the STN ceramics prepared by the CON method were almost the same except at x=0, which indicated that the dielectric constant at room temperature was independent of Nb composition x.

5.3.1.3 Summary

$Sr_2(Ta_{1-x}Nb_x)_2O_7$ ceramics were successfully prepared by conventional powder mixing technique. Their structural and electrical properties were systematically investigated as a function of the Nb content. The grain orientation and grain size of STN ceramics increased as a function of Nb composition x. Substitution of Ta element with Nb element played a important role in increasing grain size and grain orientation. On the other hand, the dielectric constants at room temperature were independent of the Nb composition x.

5.3.2 $Sr_2(Ta_{1-x}Nb_x)_2O_7$ Thin Films

In this experiment, the STN films were prepared by using Nb ethoxide, Ta ethoxide, and strontium acetate as starting materials, and acetic acid as solvent. At first, Ta ethoxide was mixed with Nb ethoxide in appropriate molar ratio, and then acetic acid was added as a chemical modifier as well as a solvent in the STN precursor solution. Sr

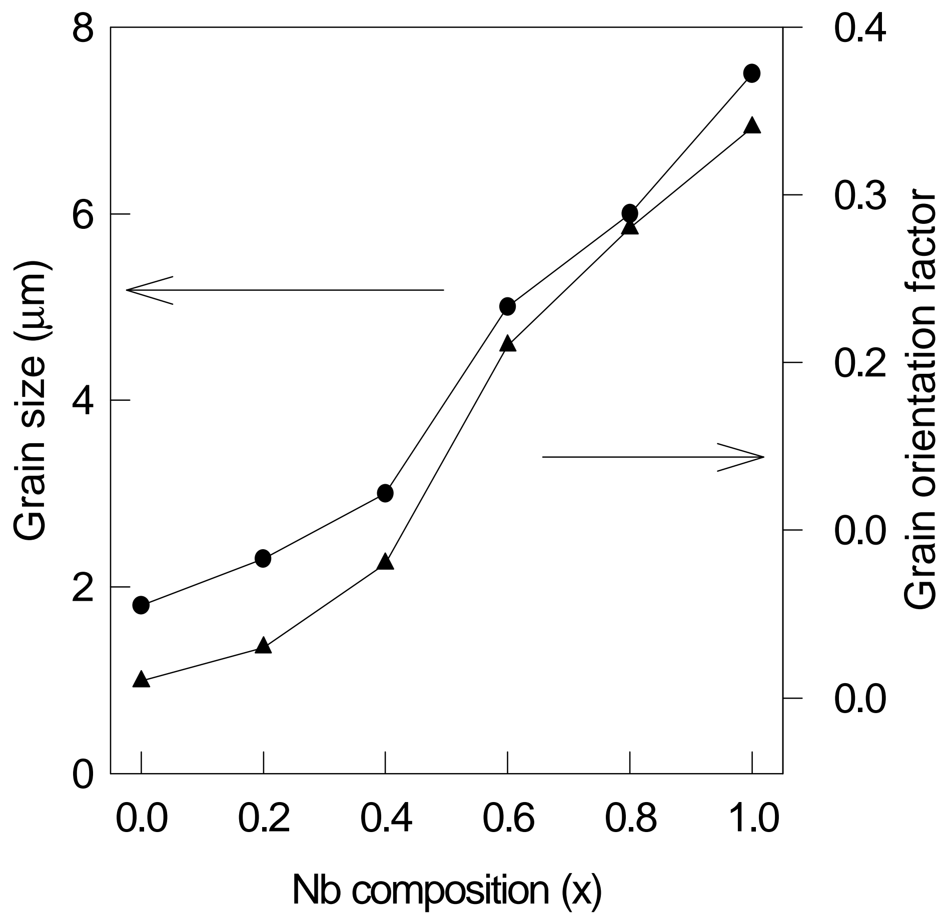

Figure 5.11 The dependence of grain size and grain orientation on the STN composition.

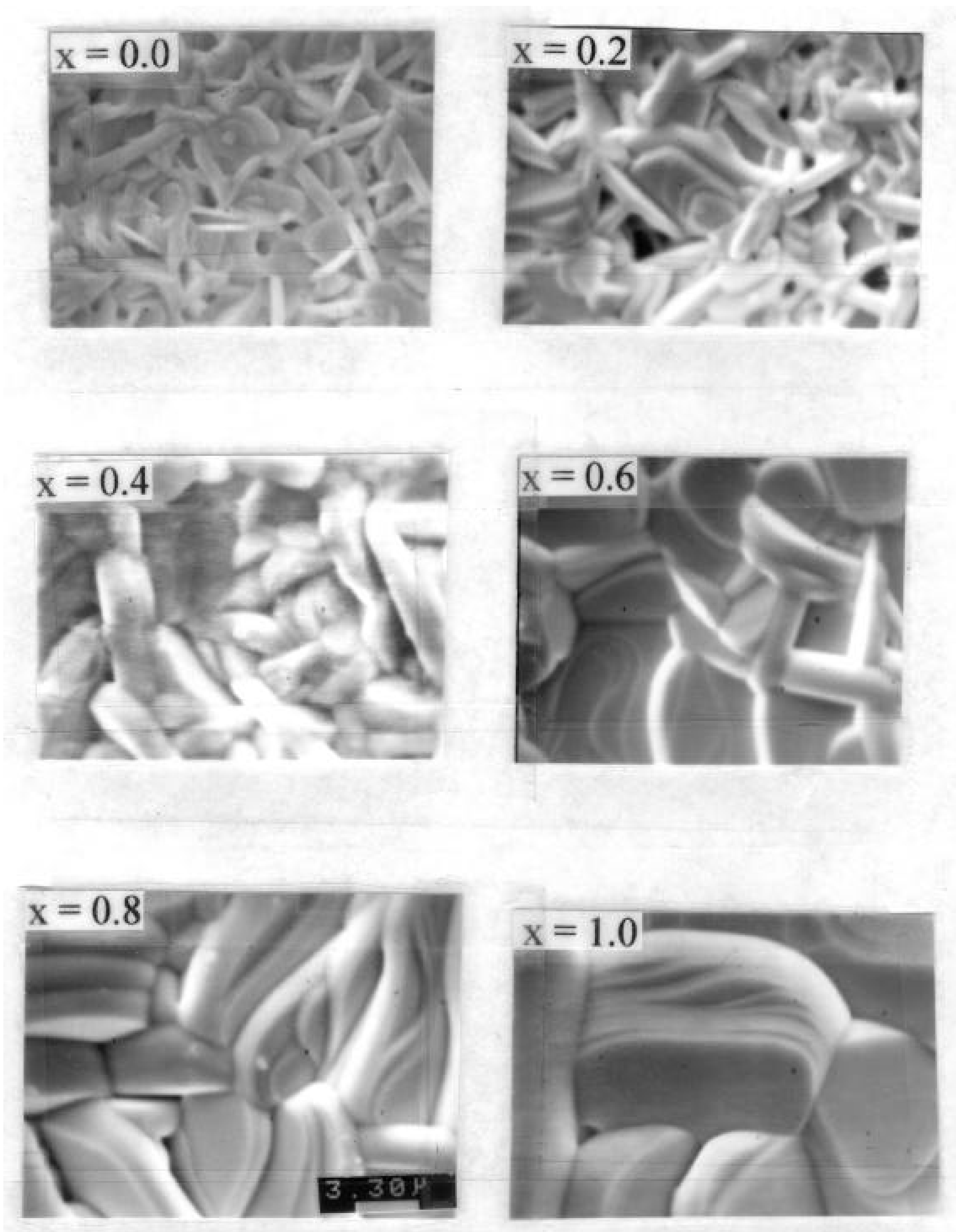

Figure 5.12 SEM pictures of STN ceramics at 1500 °C as a function of Nb content.

Table 5.1 Characteristics of $Sr_2(Ta_{1-x}Nb_x)_2O_7$ bulk ceramics sintered at 1500 °C.

	x = 0.0 $Sr_2Ta_2O_7$	x = 0.2	x = 0.4	x = 0.6	x = 0.8	x = 1.0 $Sr_2Nb_2O_7$
Curie temp. (°C)	- 107	410	735	1000	1160	1342
ε_m (at Curie temp.)		170	315	410	1105	1415
ε_r (at room temp.)	76	59	58	60	59	59
Density (g/cm^3) (% density)	6.15	5.84	5.64	5.53	5.19	4.85
Grain orientation	0.01	0.03	0.06	0.22	0.29	0.34

acetate was then put into the precursor solution. The solution was mixed for 24 h to enhance the mixing of modified precursors and produce a more homogeneous solution. The precursor solution was then deposited on Pt-coated Si, Si(100), and $Pt/IrO_2/SiO_2/Si$ substrates by spin-coating technique. The as-deposited layer was baked on a hot plate in air at 250 °C to evaporate alcohol and the residual organics. The spin-coating and baking process was repeated three times, and then the STN films were finally pyrolyzed and annealed at various temperatures ranging from 450 to 850 °C. The STN films were annealed in a pre-heated furnace under an oxygen atmosphere. After annealing, the samples were taken out and cooled under room temperature condition.

The structure development of the films was investigated by x-ray diffraction (XRD) patterns, which were recorded on a Scintag XDS 2000 diffractometer using CuKα radiation at 40 kV. The ferroelectric measurements were carried out at room temperature by using a standardized RT66A ferroelectric test system operating in a Virtual-Ground mode. For electrical measurements, Pt electrodes were deposited at room temperature on the top surface of the films through a shadow mask by rf sputtering. The area of circular dots was measured as 0.00052 cm^2.

Figure 5.13 shows the XRD patterns of STN films annealed at 850 °C on Si(100) substrate as a function of composition. Using the MOD technique, it was possible to obtain polycrystalline STN films at an annealing temperature of 850 °C. The dielectric properties of STN films were measured in terms of small signal dielectric constant and dissipation factor. The STN films prepared on Pt-coated Si substrates at 850 °C showed the dielectric constants and dissipation factors at an applied frequency of 100 kHz as around 43 - 48 and 0.021 -0.055, respectively. The effect of composition on dielectric constants was shown in Figure 5.14. The STN films exhibited lower dielectric constants than the bulks, and the low dielectric constants were not dependent upon the composition,

as observed in STN bulks. The ferroelectric properties were investigated for the STN films on $Pt/IrO_2/SiO_2/Si$ and Si(100) substrates. Unfortunately, the hysteresis loop was not found for the STN films, which might be attributed to the stress generated from the substrate processing or lattice mismatching.

5.4. SUMMARY

$A_2B_2O_7$ type ferroelectric thin films such as $Sr_2Nb_2O_7$ and $La_2Ti_2O_7$ were successfully developed on Pt-coated Si and Si(100) by a metalorganic deposition (MOD) technique. Using the MOD technique, it was possible to obtain polycrystalline $Sr_2Nb_2O_7$ films at an annealing temperature of 850 °C via intermediate phase whose composition is close to $Sr_{0.8}NbO_3$. Randomly oriented $La_2Ti_2O_7$ thin films were crystallized at 750 °C without any intermediate phase. The dielectric constants of $Sr_2Nb_2O_7$ and $La_2Ti_2O_7$ films were 46 and 48, respectively, at a frequency of 100 kHz. $Sr_2(Ta_{1-x}Nb_2)O_7$ bulk ceramics and thin films were fabricated for investigating the structural and electrical properties of the solid solutions. Very strong (0k0) grain orientation was observed for polycrystalline STN ceramics when Nb content is larger than 0.6, and then decreased as Ta content increased. The grain size also decreased with increasing in Ta content. The dielectric constants of STN bulk ceramics were around 60, and almost independent of the composition. STN thin films were prepared on Si(100), Pt-coated Si, and $Pt/IrO_2/SiO_2/Si$ substrates at 850 °C, and displayed a random orientation. The dielectric constants of the STN films were around 45, which was lower than the bulk values. The ferroelectricity of the STN films was not observed at this point, which might be attributed to the stress generated from the lattice mismatching.

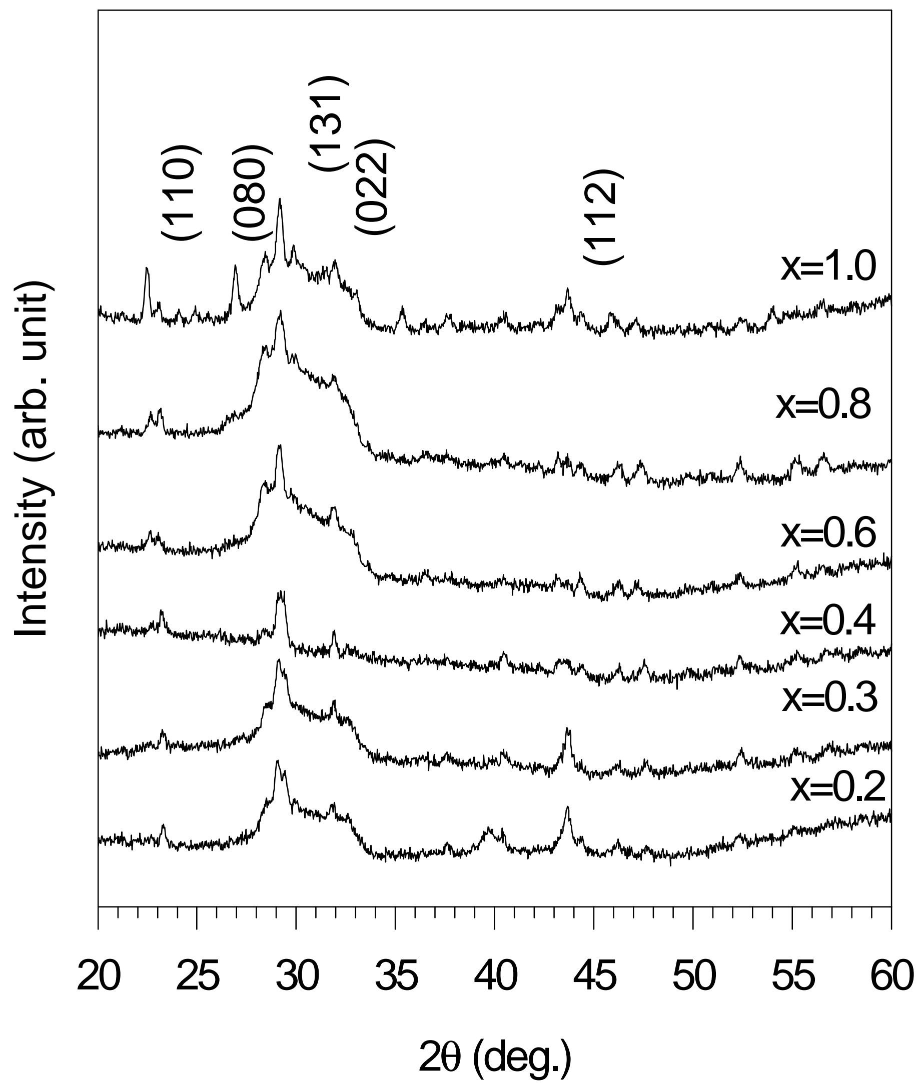

Figure 5.13 XRD patterns of STN films on Si(100) substrate annealed at 850 °C.

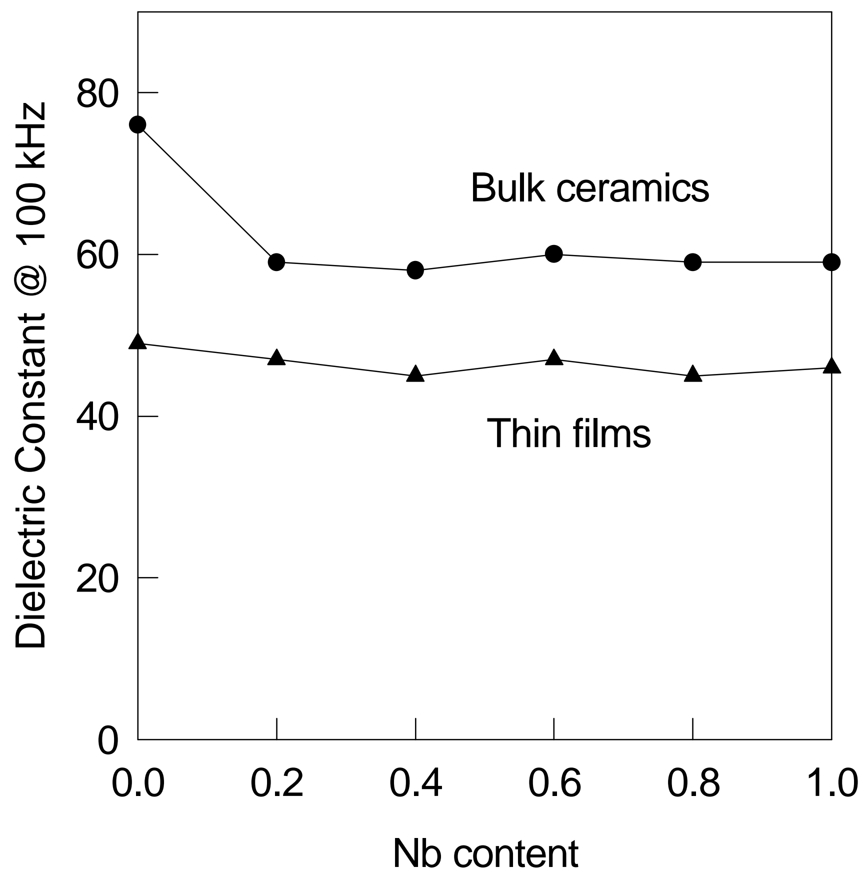

Figure 5.14 Dielectric constants of STN bulk and thin films.

5.5 REFERENCES

1. S. Shinharoy, H. Buhay, D. R. Lampe, and M. H. Francombe, *J. Vac. Sci. Technol. A*, 10(4), (1992), 1554-1561
2. J. F. Scott, *Phys. World* (February 1995), 46.
3. S. Y. Wu, *IEEE Trans. Electron Devices*, 21, (1974), 499.
4. Y. Nakao, T. Nakamura, A. Kamisawa, H. Takasu, N. Soyama, T. Atsuki, and K. Ogi, Jpa. *Jpn. J. Appl. Phys. Part I*, 33, (1994), 5265.
5. H. Buhay, S. Sinharoy, M. H. Francombe, W. H. Kasner, J. Talvacchio, *Proc. of the 3rd ISIF*, (1991).
6. M. Bogdon, S. Sinharoy, and A. J. Noreika, *J. Vac. Sci. Techol.* A9, (1991) 2420.
7. W. J. Takei, N. P. Formigonic, and M. H. Francombe, *J. Vac. Sci. Technol.*, 7, (1970) 442.
8. H. Buhay, S. Sinharoy, W. H. Kasner, M. H. Francombe, D. R. Lampe, and E. Stepke, *Appl. Phys. Lett.*, 58, (1991), 1470.
9. S. Nanamatsu, M. Kimura, K. Doi, and M. Takahashi, *J. Phys. Soc. Japan*, 30, (1971), 300.
10. S. Nanamatsu, M. Kimura, and T. Kawamura, *J. Phys. Soc. Japan*, 38, (1975), 817.
11. N. Ishizawa, F. Marumo, T. Kawamura and M. Kimura, *Acta Cryst.*, 1331, (1975), 1912.
12. G. A. Smolenskii, V. A. Isupov and A. I. Agranovskaia, *Soviet Physics-Doklady*, 1, (1956), 300.
13. S. Nanamatsu, M. Kimura, K. Doi and M. Takahashi, *J. Phys. Soc. Jpn.*, 30, (1971). 300.

14. M. Kimura, S. Nanamatsu, K. Doi, S. Matsushita and M. Takahashi, *Jap. J. Appl. Phys.*, 11, (1972), 904.
15. R. H. Arendt, J. H. Rosolowski, and J. W. Szmaszek, *Mater. Res. Bull.*, 14, (1979), 703.
16. J. K. Yamamoto and A. S. Bhalla, *Mater. Lett.*, 10, (1991), 497.
17. R. W. Vest and J. Xu, *IEEE trans. UFFC,* 35, (1988) 711.
18. F. K. Logering, J. *Inorg. Nucl. Chem.*, 9, (1959), 113.